ICARUS **130,** 449–460 (1997)
ARTICLE NO. IS975830

New Composite Spectra of Mars, 0.4–5.7 μm

Stéphane Erard

Institut d'Astrophysique Spatiale, CNRS, Université Paris-11, bâtiment 121, 91405 Orsay Campus, France
E-mail: Erard@ias.fr

and

Wendy Calvin

United States Geological Survey, Flagstaff, Arizona 86001

Received April 21, 1997; revised July 23, 1997

About 15 areas were observed in the equatorial regions of Mars by the infrared spectrometers IRS (Mariner 6 and 7) and ISM (Phobos-2). The comparison between the spectra shows a remarkable consistency between two data sets acquired 20 years apart and calibrated independently. This similarity demonstrates the accuracy of ISM calibration above 2 μm, except for a possible stray light contribution above 2.6 μm, on the order of ~1–2% of the solar flux at 2.7 μm. Most differences in spectral shapes are related to differences in spectral/spatial resolution and viewing geometries. No important variation in surface properties is detected, except for a spot in southern Arabia Terra which has a much deeper hydration feature in IRS spectra; differences in viewing geometries and spatial resolutions do not seem to account for this difference that could result from shifting or dehydration of surface materials. Composite spectra of several types of bright and dark materials are computed by modeling the thermal emission and are completed with telescopic spectra in the visible range. Modeled reflectance in the 3.0–5.7 μm range is consistent with basalts and palagonites. The bright regions and analog palagonite spectra are different from hematite in this range, but resemble several phyllosilicates. We infer that (1) although hematite dominates the spectra in the 0.4- to 2.5-μm range, the silicate-clay host is spectrally active beyond 3 μm and can be identified from this domain; (2) phyllosilicates such as montmorillonite or smectite may be abundant components of the martian soils, although the domain below 3 μm lacks the characteristic features of the most usual terrestrial clay minerals. © 1997 Academic Press

Key Words: **infrared observations; Mars surface; spectroscopy; planets surfaces.**

INTRODUCTION

Spectroscopic measurements in the near-infrared are key observations to understand planetary mineralogy and retrieve compositional information on a global scale. The 0.5- to 2.5-μm range makes it possible to study ferric/ferrous minerals, while alteration salts are best studied from the 2.5- to 5-μm domain. Those two spectral ranges are particularly useful to understand the formation and evolution of the martian surface (e.g., Singer 1985, Roush *et al.* 1993, Soderblom 1992).

Although this whole spectral domain has not yet been covered by a single instrument, IRS on board Mariner 6 and 7 and ISM on board Phobos-2 performed observations of quality that cover complementary sub-ranges. The present comparison between the two data sets is intended to assess ISM calibration's accuracy at longer wavelengths, to check the permanency of shallow spectral features, and to search possible differences in areas observed by the two instruments. Composite reflectance spectra are presented here. Such spectra are useful not only to understand surface mineralogy, but also to prepare future observations; in accordance with a spectral model they allow an estimate of the magnitude of the expected signal and of the signal-to-noise ratio required to perform interesting new observations. The imaging spectrometer OMEGA that was lost with the Mars-96 mission was expected to acquire data from 0.5 to 5.2 μm, with a spatial resolution of 350–1500 m. These observations would have addressed fundamental questions regarding the evolution of the planet, including the development of organic chemistry and the possible biological evolution, and would have also allowed a global survey of mineral resources in view of robotic and human exploration. Therefore OMEGA or a similar instrument should eventually be flown on a future mission to Mars, probably in 2001 (Surveyor 2001 orbiter) or 2003 (Mars Express ...). Observations of this sort would benefit from a spectral model of the planet. The combined IRS and ISM data give access to a wider spectral range than any previously published spectrum of Mars (e.g., Mustard and Bell 1994, Singer *et al.* 1979) and provide a good basis for such a model.

0019-1035/97 $25.00

DATA SETS, UNCERTAINTIES, AND CONDITIONS OF OBSERVATION

The near-IR channel of IRS (Mariner 6 and 7) performed spectral measurements in the 1.9- to 6.0-μm range. Spectral information was acquired through a rotating filter (CVF), with a spectral resolution of about 1.5%. During the 10 s acquisition time the spacecraft moved on its orbit, so that the two extremities of the spectra do not exactly correspond to the same location; the corresponding footprint is $\sim 200 \times 100$ km^2 for a IFOV of $\sim 200 \times 15$ km^2. Spectra were measured in two segments with overlapping spectral ranges (1.9–3.7 μm and 3.0–6.0 μm); these segments are integrated after independent spectral and flux calibration, as described by Calvin 1997. Calibration is performed at short wavelengths (<3.3 μm) by dividing out a spectrum of the Sun reflected off the spacecraft on board Mariner 6. The relative uncertainty ($\sim$10% in general) is limited by the accuracy of this measurement and by poor knowledge of the transfer function for Mariner 7 spectra; possible OH absorptions in the spacecraft paint reflecting the Sun may result in a larger systematic error around 3 μm. At longer wavelengths (>3.3 μm) ground based observations of black bodies at various temperatures are used to estimate the transfer function. The instrumental noise ranges from 0.5 to 10%. A wavelength calibration uncertainty of about 2% remains in the spectra used here. Other measurements exist up to 14.4 μm but are not used in this study. A brief description of instrument and data calibration is given by Calvin 1997.

The imaging spectrometer ISM (on board Phobos-2) spanned the spectral range from 0.77 to 3.14 μm. All spectral measurements were acquired at the same time step and correspond to a given area on the surface ($\sim 20 \times 20$ km^2). The spectral range was sampled in 128 channels with two PbS arrays in staggered rows; this detector technology resulted in a slight registration discrepancy between two sets of 64 spectral channels. To minimize this problem we use only the set of channels with the most accurate calibration, which yields a spectral resolution of $\sim$5%. Up to 2.6 μm, data are calibrated using telescopic observations by McCord *et al.* 1982; both telescopic and ISM spectra used for calibration are taken in areas different from those studied here. Absolute uncertainty (i.e., on the average reflectance) is about 15%; relative uncertainty (i.e., on channel ratios) is determined by reference spectra and is of the order of 3%. Above 2.6 μm, calibration relies on both ground-based calibrations and a spectral model for Phobos described by Erard *et al.* 1994; uncertainty is thus larger, on the order of 10–20%. The instrumental noise ranges from 0.3 to 3% of the signal and allows survey of spatial variations with this accuracy. Instrument functioning is described by Bibring *et al.* 1990; details about the current calibration procedure and consistency check are provided by Mustard *et al.* 1993 and Erard *et al.* 1994; a complete technical documentation will be distributed on CD with the ISM data base (Erard 1997).

The two data sets were acquired almost 20 years apart, in different martian seasons: $L_S = 200°$ for IRS (northern hemisphere fall) and 0° for ISM (northern hemisphere spring). All data were acquired from noon to early afternoon, except ISM observations of Arabia that were performed in the late morning (around 10 o'clock). Atmospheric opacity was very low during ISM observations ($\sim$0.2 at 1.9 μm, e.g. Chassefière *et al.* 1995, Moroz *et al.* 1991), with little or no dust activity reported. Opacity during IRS observations is estimated to be 0.3 to 0.5 at this wavelength, based on opacity of 0.2 at 9 μm (T. Martin, personal communication) coupled with the visible/thermal infrared opacity ratio of 2 to 2.5 (Clancy *et al.* 1995, Martin 1986) and the visible/near infrared ratio of 1 to 1.5 derived from ISM (Erard *et al.* 1994). In both cases the atmosphere was clear; the slightly larger opacity during IRS observations is expected to result mainly in a steeper negative spectral slope due to aerosols backscattering.

COMPARISON OF SPECTRAL MEASUREMENTS

Most IRS observations were performed at high southern latitudes during a single flyby, while ISM acquired data only in the equatorial regions from a circular orbit. However, IRS and ISM observations overlap in two areas: first from Lunae Planum to Margaritifer Sinus through Aurorae Planum and Capri-Eos chasmata (Mariner 6 observations) and second, in southern Arabia Terra (Mariner 7 observations). The two data sets were registered independently on the surface, with an accuracy on the order of 0.5° (Fig. 1). Observations in these areas were performed under large incidence and emergence angles by both instruments, but under very different phase angles ($<5°$ for ISM, $>50°$ for IRS; see Table I). Last, thermal emission is negligible in ISM spectral range but not in IRS's, and must be accounted for. In Figs. 2, 3 and 4, IRS spectra are calibrated according to the procedure developed by Calvin 1997: the radiance is computed from the signal, then it is divided by the sum of a solar spectrum and the estimated thermal emission. The solar spectrum used is a measurement by IRS on board Mariner 6 at short wavelengths and a simulation by a Planck function at longer wavelengths; thermal emission was estimated by fitting a black body curve to the radiance measured. This procedure provides radiance factors at short wavelengths where thermal emission of the surface is negligible; above 3.5 μm IRS signal increases toward 1 as the signal becomes dominated by the emitted component.

We take advantage of the higher spatial resolution of ISM to test whether the areas spanned by IRS are uniform. About 15 ISM spectra are integrated in the central part of each IRS footprint. The mean and standard deviation

of these spectra are computed in each spectral channel. Wherever the maximum standard deviation is large outside the atmospheric bands ($\geq$10% in general) the area is considered nonuniform and is discarded (Table I). This procedure insures that IRS's IFOV remains within a spectrally homogeneous unit as spectral data is acquired; in this case we can compare the mean ISM spectrum with the corresponding IRS spectrum. A simple superposition of the spectra shows that consistent features are present in both data sets (Fig. 2). The agreement in absolute reflectance is always better than 15% below 2.6 μm, with IRS spectra always brighter than ISM spectra (Table I). The discrepancy is within the usual limits of photometric accuracy; the systematic effect could be ascribed to calibrations or different viewing geometries rather than to changes in surface or atmospheric properties. Other differences in spectral shapes are related to better signal-to-noise ratio in ISM spectra (smoother) and to better spectral resolution of IRS data (the atmospheric bands are resolved by IRS, not by ISM).

Figure 3 shows merged spectra, with IRS data scaled to ISM level at 2.45 μm. While reflectance calibration of both data sets is completely independent, the spectra appear in very good agreement in the range of overlap, i.e., from 1.9 to 3.2 μm. Inflexions at 2.4 and 2.52 μm in particular are similar; another inflexion at 2.95 μm found in IRS spectra is also visible in ISM data. No large variation of spectral properties is observed (with the possible exception of Arabia detailed below), which implies a relative permanency of the observed regions during that period.

The main differences consist in:

- deeper atmospheric bands at 1.9–2.15 μm and 2.65–2.85 μm seen by IRS, related to larger observation angles. The difference in band profiles is related to spectral resolution and is strongly reduced when IRS data are integrated to ISM resolution (Fig. 4).
- a narrow CO_2 atmospheric feature at 2.15 μm present in IRS spectra, not in ISM. This feature actually disappears on convolved IRS data (Fig. 4).
- a deeper H_2O band at 2.65 μm in ISM spectra, due to water vapor. This may be related to a small calibration error or to a slightly different amount of atmospheric water (nearly the same amount is expected for these seasons at this latitude from Viking's MAWD experiment, Jakosky and Farmer 1982).
- a substantially higher reflectance level in the hydration band from 2.85 to 3.2 μm in ISM spectra.
- a very small and narrow band at $\sim$2.2 μm was identified by Murchie *et al.* 1993 in ISM data and attributed to metal–OH vibrations in hydroxylated silicates; IRS signal-to-noise ratio is too low to confirm this feature.
- another faint and narrow absorption in the 2.3- to 2.45-μm region is observed in both data sets, with different distributions.
- a difference in spectral slope, with a steeper negative slope in some IRS spectra. This effect is not systematic and may be related to a larger heterogeneity of the areas observed, or to a larger contribution from atmospheric scattering in IRS observations of these areas.

The features at 3.4 and 3.9 μm in the spectra of Arabia Terra are instrumental artifacts (absorptions in Mariner 7-IRS filter). The last two channels of ISM spectra are noisy and very sensitive to small variations in detector temperature; they provide inconsistent measurements between sessions.

INTERPRETATION

The feature in the 2.3- to 2.45-μm domain has been ascribed both an atmospheric (e.g., Encrenaz and Lellouch 1990, Erard *et al.* 1991) and a surface origin (e.g., Singer 1985, Clark *et al.* 1990, Calvin *et al.* 1994). This feature is observed on bright regions in both data sets. It is often present in IRS spectra of dark regions, but not in ISM. This may indicate that superficial deposits have actually shifted during the 20-year period, although this seems very unlikely without any obvious change in surface reflectance. Alternatively, seasonal or secular modifications of local material could account for this difference; in particular, adsorption or inclusion of atmospheric water in the surface layer can produce a feature at this location. Another possible explanation is that the atmospheric component of this feature is prominent and more intense because of longer atmospheric path.

The most obvious discrepancy concerns the reflectance level in the hydration band at 3.0 μm, with a band 15% deeper in average in IRS data (Table I). Ongoing restoration of the IRS data set implies that the band depth is probably underestimated, so that the difference with ISM is actually larger. The transfer function is derived from a spectrum of the Sun in reflection on the spacecraft. The reflectance was assumed to be perfectly flat in the calibration used here, but samples of the spacecraft paint appear to contain significant OH absorptions around 3.0 μm (L. Kirkland, personal communication, 1997). The difference in band depth between ISM and IRS can be ascribed mainly to the difference in phase angles: the phase function is nearly isotropic at 2.5 μm (in the continuum) because photons suffer numerous reflections in the material and lose track of the incidence direction. At 3.0 μm where absorption is very large most emerging photons have been scattered only once and hence are concentrated around the specular direction. This difference in phase function inside and outside the band results in increased spectral contrast at larger phase angles or further from the normal direction (e.g., Veverka *et al.* 1978). The martian phase function in this domain is completely unknown however, so the photometric effect cannot be quantified; hence, sea-

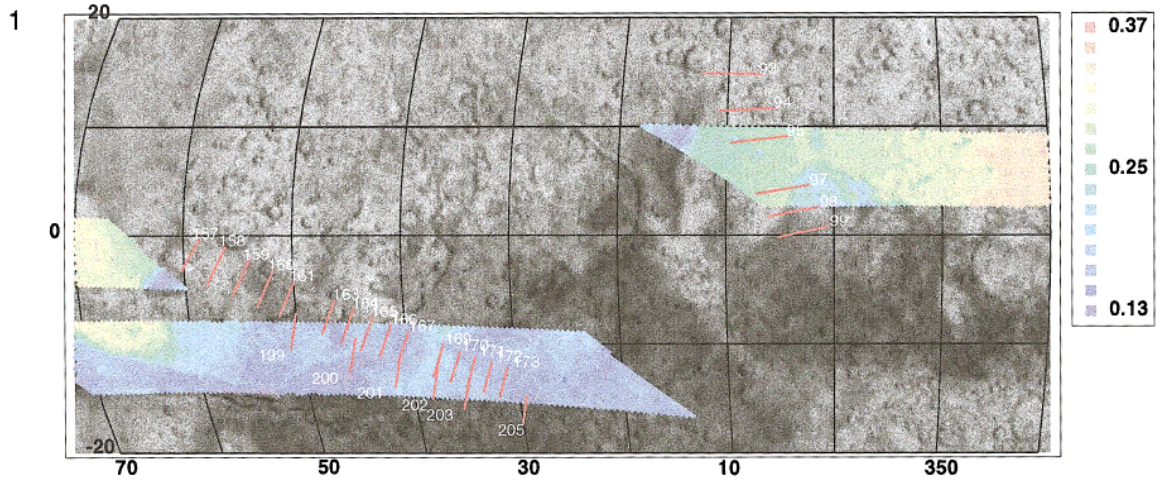
1
20
0
-20
70
50
30
10
350
0.37
0.25
0.13

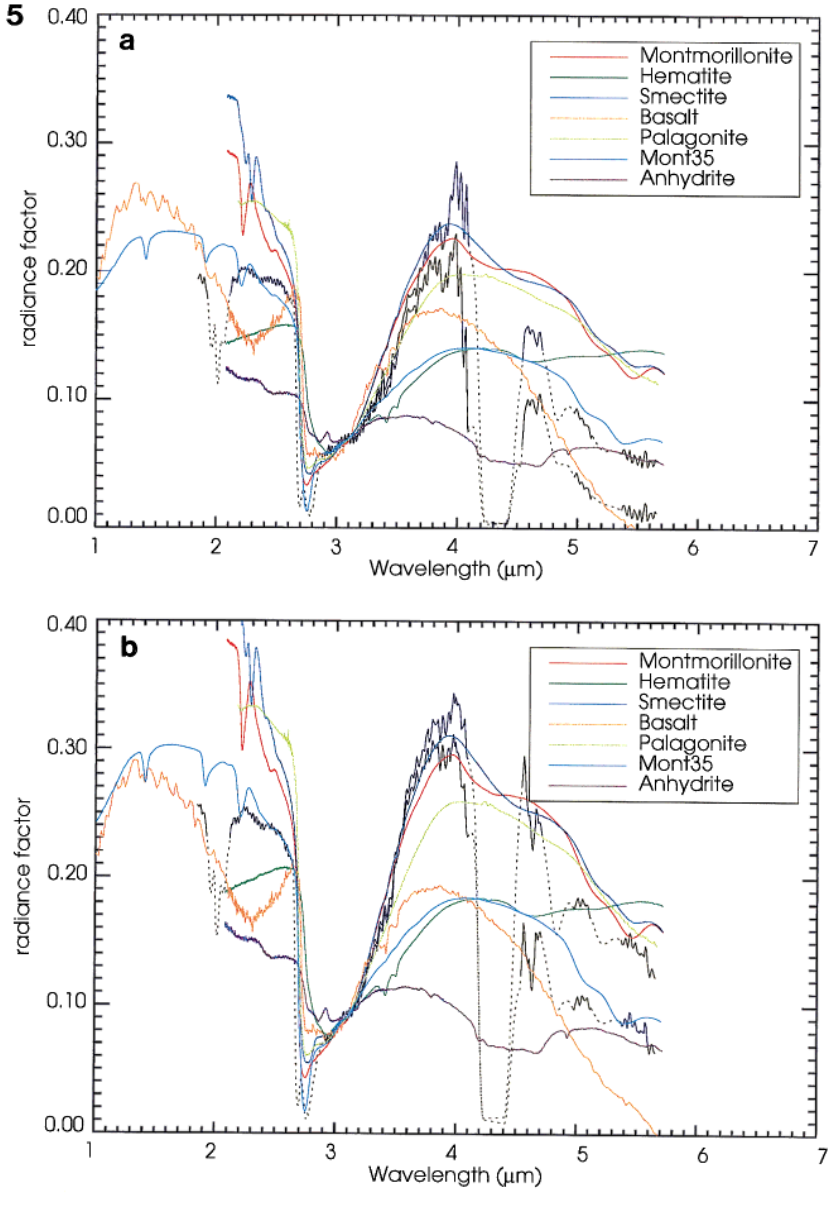
5
a
b
Montmorillonite
Hematite
Smectite
Basalt
Palagonite
Mont35
Anhydrite
radiance factor
Wavelength (μm)
0.00
0.10
0.20
0.30
0.40
1
2
3
4
5
6
7

TABLE I

IRS spectrum	Maximum dispersion	IRS/ISM at 2.44 μm	IRS/ISM at 3.05 μm	Contrast ratio	IRS			ISM		
					e	i	φ	e	i	φ
7-95	5%	1.05	0.70	0.67	67.9°	19.7°	48.4°	42°	38°	4.5°
7-97	12%	1.04	0.71	0.67	62.9°	14.6°	48.4°	37.5°	36°	1.5°
7-98	15%	0.91	0.70	0.77	60.7°	12.4°	48.4°	36°	35°	0.5°
6-157	—	—	—	—	64.0°	8.9°	55.5°	—	—	—
6-158[a]	—	0.99	0.73	0.74	61.3°	6.5°	55.5°	18.5°	25°	6.6°
6-159	—	—	—	—	63.0°	4.6°	55.5°	—	—	—
6-166	5%	1.11	0.94	0.85	44.9°	11.8°	55.5°	17.7°	16°	1.8°
6-167	5%	1.13	1.00	0.89	43.2°	13.5°	55.5°	17.5°	19.8°	2.4°
6-169	10%	1.02	0.87	0.85	39.9°	16.8°	55.5°	23.3°	20.2°	3.0°
6-170	10%	1.20	0.93	0.77	38.4°	18.4°	55.5°	25.1°	21.6°	3.5°
6-171	5%	1.02	0.86	0.84	36.9°	19.9°	55.5°	26.5°	22.5°	3.7°
6-172	3%	1.03	0.93	0.90	35.4°	21.5°	55.5°	28.5°	24°	4.1°
6-173	3%	1.01	0.92	0.90	33.9°	23.0°	55.5°	30°	26°	4.3°
6-199[b]	5%	1.22	1.08	0.89	79.3°	4.9°	83.9°	16°	15°	1.6°
6-200	10%	1.15	1.12	0.98	73.7°	10.4°	83.9°	18.4°	16.1°	2.7°
6-201	10%	1.30	1.21	0.97	69.6°	14.5°	83.9°	22.4°	18.8°	3.9°
6-202	5%	1.15	1.10	0.87	66.1°	17.9°	83.9°	26°	21.5°	4.5°
6-203	5%	1.11	1.02	0.92	63.0°	21.0°	83.9°	28.5°	23.5°	4.9°

[a] Spectra 157–159 do not overlap ISM sessions. Spectrum 158 is merged with ISM observations of a nearby area, so the ratios are only indicative.
[b] The part of the footprint that doesn't overlap the ISM image cube is in a very different geologic area, so this spectrum is probably a mixture of different spectral types.

sonal or long-term changes in surface hydration level can also contribute to the band depth variation.

In Arabia, the hydration band is much deeper in IRS spectra, even when taking into account the average difference between the two data sets (30% deeper versus 15% in average, see Table I). IRS observations in Arabia are the only ones in this work that were acquired from Mariner 7, but no large difference in filter transmission is observed between the two IRS instruments, although a calibration discrepancy cannot be excluded. The viewing geometries are not very different from what they are for Valles Marineris and do not explain the particular behavior in Arabia. Although the region appears relatively homogeneous at the time of ISM observations, it exhibits slightly different albedo patterns in Viking maps and the ISM image. Therefore, this area may have been covered at the time of IRS observations by bright hydrated material that has been dispersed or dehydrated 20 years later. This is the only area among those studied here where an important surface change is suspected, although it is not demonstrated.

Another interesting difference concerns the depth of the 2.65- to 2.85-μm CO_2 band. Careful comparisons of ISM measurements with atmospheric line models suggest that ISM reflectance could be overestimated by a factor of 5 to 10 in this band (D. Titov, personal communication, 1996). In Fig. 4, IRS spectra with similar CO_2 absorption at 2.0 μm do exhibit a deeper 2.7-μm band than ISM, although by a factor of 2–3 only (see Table II). The difference in atmospheric path lengths and a possibly stronger

FIG. 1. ISM and IRS overlapping observations, displayed on the USGS airbrush map. The red lines represent the projection of IRS's spectrometer slit on the surface at middle of acquisition. IRS footprints are in first approximation adjacent areas centered on these lines; the short wavelengths (1.9–3.75 μm) are acquired on areas north of these lines. Three ISM sessions in this region are displayed with color codes representing radiance factors at 0.9 μm.

FIG. 5. IRS spectra (a) in Margaritifer Terra (6–171, dark) and (b) in Ophir Planum (6–160, bright). Thermal emission is removed from IRS spectra under two extreme determinations of surface temperature (302–303.5 K, and 293–295 K, respectively). Higher temperature provides higher level around 3.8 μm and lower level above 4.5 μm. Corrected spectra are compared with a basalt rich in clinopyroxenes (Basalt1 from ASTER library, hemispherical reflectance), several minerals from Salisbury *et al.* 1991 (Montmor.2P_1, Hematite.1F_1, Smectite.1P_1 and Anhyd.1S_1), a palagonite spectrum from James Orenberg (personal communication), and ferryhydrite-bearing montmorillonite #35 from Bishop *et al.* 1995. Laboratory spectra are scaled to IRS level at 3.12 μm.

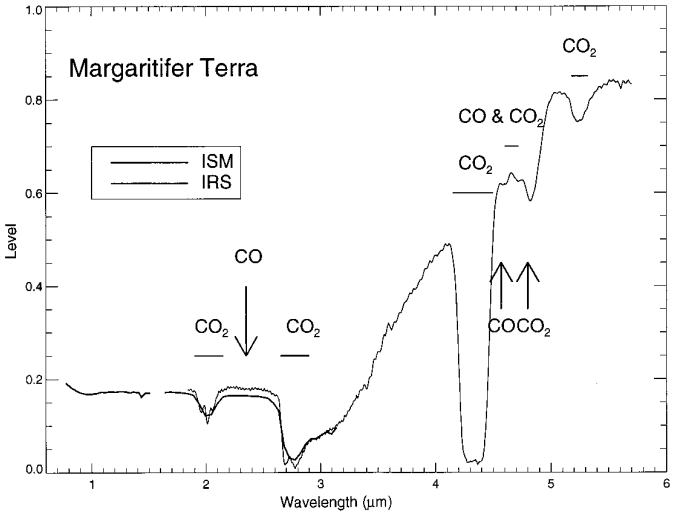

FIG. 2. Simple superposition of corresponding spectra of dark plateau material in Margaritifer Terra (IRS spectrum 6–173), with main atmospheric features indicated. The absolute levels match typically within 15%. The increase above 3.5 μm is related to planetary thermal emission. The gap from 1.51 to 1.63 μm corresponds to the limit between the two optical paths of ISM, where no measurement is made. The quantity along the *Y*-axis is the radiance divided by the sum of the solar flux and the estimated thermal emission; it is equal to the radiance factor only at short wavelengths (see text).

atmospheric scattering in IRS data make it difficult to precisely compare the reflectance levels, however. The discrepancy between the atmospheric model and IRS reflectance can be easily explained by the possible OH absorption in the spacecraft paint used as reference (see discussion in the above paragraphs). The difference with ISM reflectance could result from a systematic error in ISM calibration above 2.6 μm; in this domain the calibration relies on a spectral model for Phobos (discussed by Erard *et al.* 1994), so this possible error would affect the 2.7-μm band and the 3.0-μm regions similarly. This error can be either multiplicative (related to the transfer function) or additive. The reflectances at 3.0 μm match independent photometric observations of nearby areas under a similar geometry within 20% (data from Roush *et al.* 1992). A multiplicative calibration error of more than 20% on ISM reflectance above 2.6 μm would thus be inconsistent with reflectance at longer wavelengths. Conversely, an additive contribution corresponding to 1–2% of the solar flux would account for the mismatch at 2.7 μm and would fit within the 20% accuracy at 3.05 μm (Table II). Such an additive contribution could be related to dark current removal, to contamination of Mars spectra by stray light, or to an underestimate of the width of ISM's channels; in this latter case the level above 3 μm would not be much

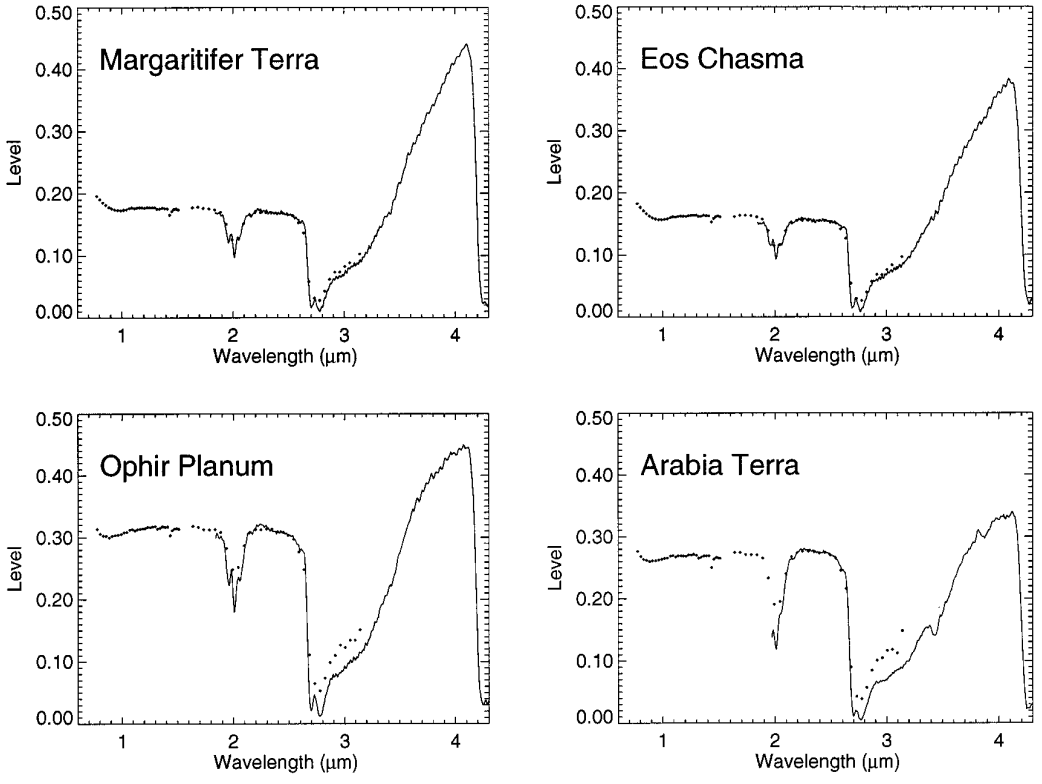

FIG. 3. Some examples of merged spectra, scaled at 2.45 μm and cut at 4.3 μm. IRS spectra (solid lines) are 6–172 (Margaritifer), 6–167 (Eos Chasma), 6–158 (Ophir Planum) and 7–95 (Arabia). The feature at 3.4 μm in the Arabia spectrum is a residual absorption in Mariner 7 filter.

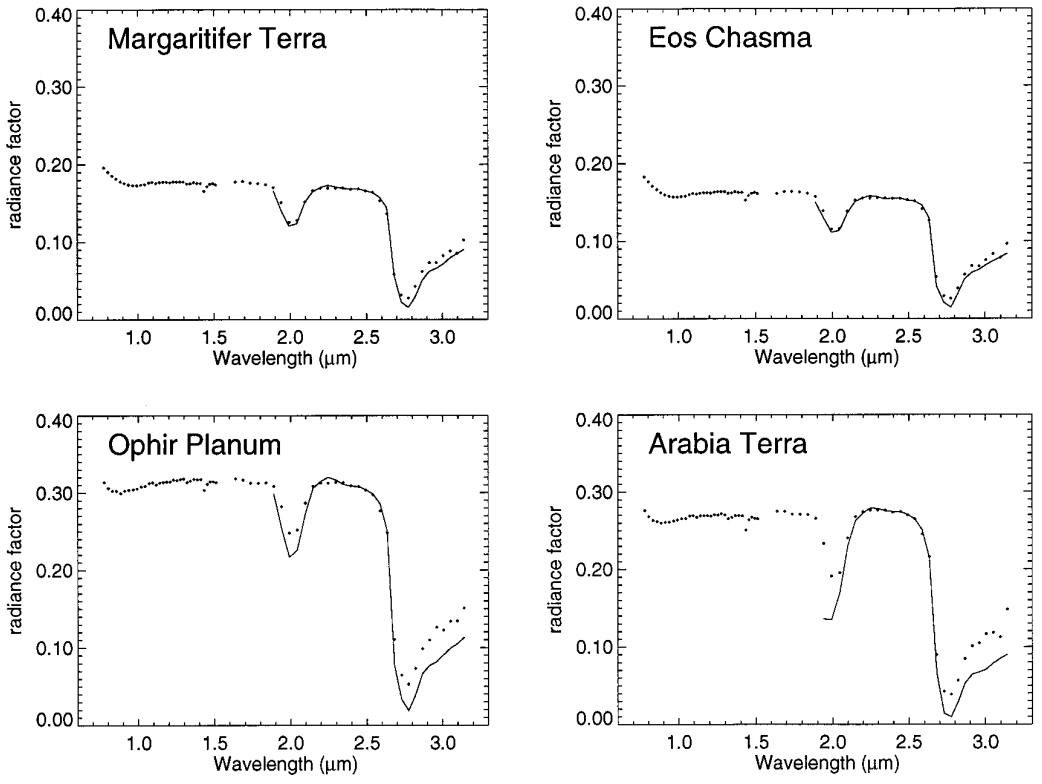

FIG. 4. Same spectra as in Fig. 3, but IRS data are convolved with ISM spectral responses.

affected. Anyway, a systematic additive error alone could not account for the difference in hydration band between the two data sets.

REFLECTANCE SPECTRA

Composite reflectance spectra in a large wavelength range are needed to understand surface mineralogy. The earliest attempt to correct thermal emission and recover surface reflectance in a narrower range was made by Moroz 1964 from telescopic observations; this work allowed the first detection of hydrated minerals in the martian soils (see the review by Soderblom 1992). At the spatial resolution of ISM and IRS several types of bright and dark material can be distinguished (e.g., Erard 1995, Erard *et al.* 1991); four spectra are presented here. These spectra almost encompass the whole range of albedo variations of martian soils. The thermal contribution to IRS measurements is removed using the model described in the Appendix; this provides an estimate of martian reflectance from 3.0 to 5.7 μm, the first one in such a large spectral range. We first discuss the application of our model, then merge IRS, ISM, and telescopic data, and present the resulting spectra.

TABLE II

Data	r_F at 2.77 μm	r_F at 3.05 μm
ISM	0.025–0.035	0.08–0.12 ± 20%
IRS	0.01–0.02	0.07–0.10
Telescopic ($\varphi \sim 25°$)[a]	0.005	0.07–0.12 ± 10%
Atmospheric model[b]	0.005–0.010	—
ISM − 0.2	0.005–0.015	0.06–0.10
ISM/5	0.005–0.007	0.016–0.02

[a] Roush *et al.* 1992
[b] Titov 1996, personal communication.

Martian Reflectance at Long Wavelength

In the model detailed in the Appendix, the major unknown is temperature. The data are first fitted between 5.0 and 5.7 μm by a black body multiplied by an estimate emissivity, which is adjusted interactively for self-consistency; in this procedure, both the absolute radiance and the spectral slope are used to determine temperature. Another criterion is the credibility of the resulting spectra. When the assumed temperature of the surface is raised, the modeled reflectance decreases around 4.0 μm and increases very quickly above the CO_2 band at 4.5 μm. Only a range of 1°–3° provides a positive reflectance at all wavelengths (Fig. 5). Temperatures determined in this study are systematically higher by 8–10 K than those published by Pimentel *et al.* 1974, in accordance with Calvin 1997 who used the same refined data calibration.

The other major source of uncertainty is atmospheric absorption, particularly on the shoulders of the bands; this is partly due to enlargement with pressure, but also to uncertainty on IRS wavelength calibration. For this reason surface reflectance cannot be accurately retrieved where strong atmospheric absorption occurs, and a model atmosphere is superimposed on the spectra of Fig. 5. Interpretation of these spectra can thus rely only on their overall shape, not on detailed features that include remaining atmospheric absorptions.

In the range of possible temperatures, all spectra present a maximum in reflectance located at 3.8–4.0 μm; a systematic drop-off at 4.0 μm, just below the CO_2 band; and a strong decrease in reflectance from 4.5 to 5.7 μm. The drop-off at 4.0–4.2 μm exists in all spectra, even when the estimate temperature is clearly too low, hence it doesn't appear to be an effect of the model. This overall spectral shape is similar to that of certain basalts, although basalts present much deeper absorptions at 2.2 μm and a more convex shape in the 3.0- to 3.8-μm range (Fig. 5). All spectra acquired by IRS outside the polar caps have an important thermal contribution, and thus none of them gives a direct measurement of the soils reflectance. Spectra acquired at higher latitude and lower surface temperature ($\sim$245 K) have been compared to the modeled reflectance spectra, and have been found consistent with them.

There is a large consensus that the bright martian regions are formed of mixtures of poorly crystalline clays, ferric oxides, and sulfates, based on chemical and dynamical considerations, Viking elemental abundances, and occurrences of these minerals in SNC meteorites. Terrestrial palagonites, which are formed by alteration of mafic volcanic glasses under low temperature, are examples of such mixtures and are actually the best spectral match of martian bright materials in the visible and the NIR. Spectral properties of palagonites are dominated in this spectral range by hematite with very short-range crystalline structure (nanophase hematite), although it is only a minor component dispersed in a silicate-clay matrix (e.g., Morris *et al.* 1989). Variations in crystallinity, particle size, and composition account for most of the variations observed in the bright regions, although some areas have distinctive spectral features around 0.9 μm indicative of bulk crystalline hematite (e.g., Bell *et al.* 1990) or other alteration minerals (e.g., Murchie *et al.* 1993).

The modeled IRS reflectance of bright regions is matched by some palagonite spectra above 3.0 μm. The spectral shape of hematite is markedly different from IRS, however: the slope in the wing of the hydration band (3.0–3.7 μm) is much less steep, there is no maximum around 4.0 μm, and the spectrum is flat longward of 4.0 μm (Fig. 5). This may indicate that martian bright regions and palagonite analogs are no longer dominated by nanophase hematite at these wavelengths but that the host material can be identified from this spectral range instead. We compared the spectra with various alteration minerals thought to be present on Mars. Among these, only phyllosilicates have properties similar to those observed in IRS reflectance spectra, in particular montmorillonite and smectite. The presence of phyllosilicates is consistent with some interpretations of Mariner 9-IRIS observations (e.g., Hunt *et al.* 1973, see discussion in Roush *et al.* 1993), with several observations of suspended dust (e.g. Pollack *et al.* 1990, Erard *et al.* 1994), with Viking biology experiments (e.g., Banin and Margulies 1983), and with SNC analyses (e.g., Gooding 1992). Crystalline clay minerals are not generally thought to be very abundant on Mars however, because they usually present several features that are not observed in martian spectra (e.g., Roush *et al.* 1993, Soderblom 1992). For instance, one of the major spectral differences between laboratory samples and Mars is the absence of a H_2O absorption at 1.9 μm on Mars; actually this feature is considerably reduced when the samples are measured under low pressure and should not be expected from clay minerals in martian environment (Bishop and Pieters 1995). Another important difference is the absence of a metal-OH absorption around 2.2–2.3 μm. However, ferric sulfate-bearing and ferrihydrite-bearing montmorillonites studied by Bishop *et al.* 1995 lack the H_2O and metal-OH bands characteristic of more usual terrestrial clay minerals and can account for the variability of the bright martian regions; several iron-rich phyllosilicates studied by Calvin and King 1997 have similar spectral properties; last, Cooper and Mustard 1997 showed that the strength of these band decreases very rapidly for very small particles, and would be almost undetectable for efficient particle size on the order of 1 μm. In summary, phyllosilicates have been disregarded so far on the basis of visible and NIR spectra; this argument does not appear very strong in the light of recent laboratory measurements. Conversely there is evidence for relatively large abundances of clay minerals, and the IRS reflectance spectra derived in the present work contain features consistent with these minerals above 3.0 μm. The fact that poorly crystallized hematite dominates the spectral properties of martian materials in the visible and NIR, but not at longer wavelengths, could be related to different particle sizes of the various mineral phases, or to coating effects such as those described by Singer and Roush 1983.

Composite Reflectance Spectra

The darkest areas observed by IRS in the selected regions are located in eastern Valles Marineris and correspond to both plateau and chasma materials. Eos Chasma comprises some of the darkest areas of the planet, but spectral properties observed by ISM indicate that they are not representative of the average dark terrains (strong mafic absorption but strong hydration features, see Erard *et*

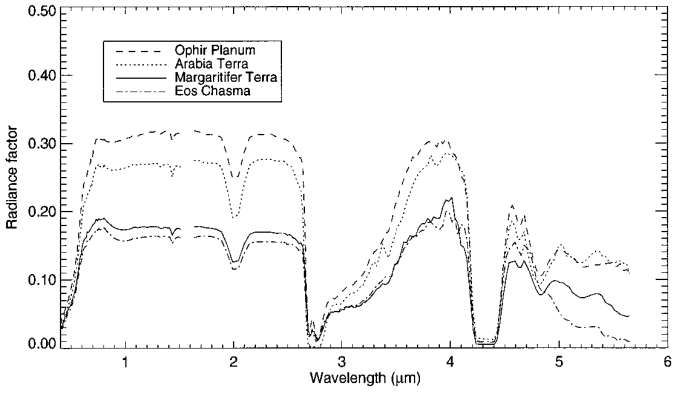

FIG. 6. Composite reflectance spectra of dark and bright areas. The visible data are from telescopic observations. Telescopic and IRS data are smoothed with a three-point convolution and merged at 0.83 μm and 2.45 μm. IRS spectra used are 6–158 (Ophir), 7–95 (Arabia), 6–167 (Eos Chasma) and 6–172 (Margaritifer Terra). In the Arabia spectrum, the feature at 3.4 μm is an artifact and the reflectance from 4.5 to 4.7 μm is arranged as described in the Appendix.

al. 1991). A spectrum of more typical dark plateau material, acquired in Margaritifer Terra south of the canyons, is also included in Fig. 6. These spectra correspond respectively to chaotic material and unit Npl1 according to Scott and Tanaka 1986.

IRS brightest spectra are located in ISM Arabia image cube. If this area has been modified between the observations as discussed above, the Arabia composite spectrum in Fig. 6 could be a mixture of bright and intermediate bright terrains. Murchie *et al.* 1993 suggested that this area is compositionaly different from most bright areas of the planet. The two data sets do not overlap on the more typical region of Tharsis, so a spectrum was composited using IRS observations of Ophir Planum (east of Juventae Chasma) and ISM observations of a similar material on the western side of the chasma. Both bright spectra fall in units Npl1 and Npl2 on the geologic map. This material is among the brightest found on Mars.

Selected bright and dark spectra have been merged with telescopic data acquired by Bell in August 1988 (from Mustard and Bell 1994, who discuss the agreement with ISM observations) and scaled to ISM level at 0.83 μm (Fig. 6). Visible observations are taken in regions with similar properties in this spectral range: the brighter spectra are completed with visible data from Tharsis and the darker ones with data from Oxia Palus (respectively spot 27 and 22 from Mustard and Bell). IRS and visible data are smoothed with a 3-point convolution to increase signal-to-noise ratio; the resulting spectral resolution is still better than ISM's.

The most obvious features in spectra of bright materials are a shallow absorption centered from 0.85 to 0.92 μm ascribed to ferric oxides and a very deep band around 3.0 μm related to hydrated minerals, corresponding to about 1% H_2O in mass. The 0.85-μm band, together with weak inflexions at 0.47, 0.53, and 0.56 μm and a small feature at 0.6–0.7 μm provides evidence for poorly crystallized hematite as a spectrally dominant component of bright materials (e.g., Bell 1992). Where the ferric absorption occurs near 0.9 μm, such as in the Arabia spectrum in Fig. 6, Murchie *et al.* 1993 suggested the presence of another ferric component (goethite, ferrihydrite, or jarosite) rather than a mixture with a pyroxene; ferrihydrite-bearing montmorillonites could also account for such absorptions (Bishop *et al.* 1995). Several subdued features have been observed at 2.2 and 2.3–2.4 μm in various data sets and were interpreted as evidence for alteration minerals. Other weak absorptions have been identified at longer wavelengths in bright regions, including bands at 5.2–5.4 μm (Calvin *et al.* 1994, ascribed to hydrous carbonates) and 4.5 μm (Blaney and McCord 1995, ascribed to sulfates). As discussed in the previous section, the overall spectral reflectance above 3.0 μm is more consistent with montmorillonite or smectite, rather than hematite. If the martian bright dust is actually similar to terrestrial palagonites, this would indicate that the composition of the silicate-clay host can be identified from this spectral domain.

At ISM spatial resolution, dark materials appear to contain abundant concentrations of relatively pristine mafic volcanic materials. They were interpreted from ISM spectra as mixtures of low- and high-calcium pyroxenes by Mustard and Sunshine 1995. The spectrum of Eos Chasma in Fig. 6 appears richer in high-calcium pyroxene, with characteristic absorptions at 0.95 and 2.25 μm, while the spectrum of Margaritifer Terra seems richer in low-calcium pyroxene, with absorptions centered at slightly lower wavelengths; a ferric component may also be present in this region, with a faint absorption centered around 0.85 μm. Although the 3.0-μm hydration band is very deep, it is much weaker than on bright regions when observed at zero phase angle; this band depth certainly depends on photometric effects and particle size however, and does not necessarily imply that water content be much lower in dark areas. Dark regions usually present steeper negative spectral slopes in the near-infrared that have often been ascribed to differences in particle size and surface mineralogy. Erard *et al.* 1994 showed that scattering by airborne particles provides a large component added to the surface reflected light, with a strong negative slope. The relative contribution of atmospheric scattering is thus larger on darker areas, and spectral slope is therefore not simply related to surface properties.

CONCLUSION

The comparison between corresponding spectra shows a remarkable consistency between two data sets acquired 20 years apart and calibrated independently. This similarity

demonstrates the accuracy of ISM calibration above 2 μm, as Mustard and Bell 1994 demonstrated at shorter wavelength.

The match in absolute reflectances is very good, on the order of the usual photometric accuracy (10–15%). Most differences in spectral shapes can be related to differences in spectral resolution and viewing geometries. Uncorrected stray light may contribute to ISM reflectance level above 2.6 μm, and would represent ~1–2% of the solar flux at 2.7 μm. Some spectra in areas near Valles Marineris apparently contain a stronger contribution from atmospheric scattering and have probably been acquired by IRS through a more dusty atmosphere. Systematic differences in the strength of the hydration feature at 3 μm are ascribed mainly to different phase angles. One area in southern Arabia Terra has a much deeper hydration feature in IRS data; differences in viewing geometries and spatial resolutions do not seem to account for this difference that could result from shifting or dehydration of surface materials. Apart from this region, no important variation in surface properties is detected.

Spectral modeling of IRS spectra provides what is apparently the first reflectance estimate of the martian equatorial regions in the 3.0- to 5.7-μm range. In this domain, reflectance spectra exhibit features that are consistent with Ca-rich basalts and some palagonites. The bright regions and analog palagonite spectra are different from the hematite spectra we had, but resemble several phyllosilicates. We infer that (1) hematite no longer dominates the spectra beyond 3.0 μm, but the silicate-clay host can be identified from this domain; (2) phyllosilicates such as montmorillonite or smectite may be abundant components of the martian soils, although the domain below 3 μm lacks the characteristic features of the most usual terrestrial clay minerals. Further comparisons with laboratory spectra will be presented in a future paper. Composite reflectance spectra of several bright and dark regions are computed from 0.5 to 5.7 μm, including telescopic data of similar areas acquired 6 months before ISM observations. These spectra will be used as an input to a spectro-photometric model of Mars. The purpose of this model will be to estimate the signal expected from future space borne imaging spectrometers, scheduled for 2001 or 2003.

APPENDIX

IRS spectra used in Figs. 2 and 3 are ratios of the measured radiance by the solar flux plus an estimated thermal component. Although it conserves the shape of narrow absorption bands, this quantity approaches 1 at long wavelengths as the reflected solar flux becomes negligible. For practical applications such as planetary flux modeling, the reflected/scattered and the emitted contributions must be known independently. Separating them requires modeling the measured signal. Although a physical model exists that describes both reflectance and emittance from a surface (Hapke 1993), its application to Mars would make sense only if atmospheric scattering were also modeled. In addition Hapke's model requires fitting a number of free parameters, which is very uncertain with so little data. Assuming a simple Lambertian behavior in emission as we do here is much simpler and should yield a similar accuracy (on the order of 10–20%).

The radiance measured by the instrument in a given direction (i, e, φ) writes

$$L_\lambda(i, e, \varphi) = r_F(i, e, \varphi)\frac{E_S}{\pi R^2}A(\mu_0, \mu) + B_\lambda\varepsilon(e)A(\mu) \quad (W\,m^2\,sr^{-1}\,\mu m^{-1}),$$

where B_λ is the black body radiance at surface temperature T, $E_S(\lambda)/R^2$ is the solar irradiance at Mars distance ($W\ m^2\ \mu m^{-1}$), r_F and $\varepsilon(e)$ are the radiance factor and the directional emissivity of the surface (both dimensionless), and $A(\mu_0, \mu)$ is the overall atmospheric transmittance.

The transmittance $A(\mu_0, \mu)$ is estimated by a synthetic spectrum computed for 2 airmasses logarithmically scaled to the depth of the CO_2 band at 2.0 μm; transmittance between the surface and the spacecraft $A(\mu)$ is then computed from geometrical considerations. Surface temperature is determined by fitting the calibrated flux at higher wavelengths with this model. The directional emissivity is estimated assuming a Lambertian behavior. In a particulate medium of isotropic scatterers, hemispherical emissivity is related to reflectance at each wavelength by Kirchhoff's law as

$$\varepsilon_h = 1 - r_S,$$

where r_S is the spherical reflectance (or bihemispherical reflectance; e.g., Hapke 1993, p. 374). For a Lambertian surface, the directional emissivity is constant ($\varepsilon(e) = \varepsilon_h$) and r_S is equal to the normal albedo p_N, i.e., to $r_F/\cos i$ (this quantity doesn't depend on incidence). This leads to

$$r_F(i, e, \varphi) = \frac{L(i, e, \varphi) - B_\lambda A(\mu)}{\frac{E_S}{\pi R^2}A(\mu_0, \mu) - \frac{B_\lambda A(\mu)}{\mu_0}}.$$

This procedure assumes a good absolute accuracy of measurements; however, temperature determination does not rely only on the absolute radiance (see text), and the shape of the resulting spectra remains consistent for small variations of the absolute level. Atmospheric transmittance is the other main source of uncertainty and must be taken into account. Finally, since the radiance factor is actually derived for a non-Lambertian surface, the estimated emissivity still varies with emergence (which attenuates the effect of the Lambertian assumption) but also slightly with incidence, which has no physical sense (see the discussion of a similar problem in Moersch and Christensen 1995). The inaccuracy associated with this estimate emissivity becomes large when the two quantities to be ratioed in the above equation change sign, i.e., in the spectral domain where thermal emission and scattered radiance are nearly equal. For most of the spectra processed here this change of sign actually occurs around 4.3 μm and is concealed by the CO_2 band. For the Arabia spectra the combination of temperature and albedo is such that it occurs at 4.5 μm, and the estimate reflectance is very unstable; in Fig. 6, the domain from 4.5 to 4.7 μm is copied from the Ophir spectrum and scaled to the average level in Arabia.

ACKNOWLEDGMENTS

Stéphane Erard was partially supported by the French Programme National de Planétologie, and Wendy Calvin was supported in part by NASA Planetary Geology and Geophysics program. This paper benefited from helpful reviews by John Mustard and Vassili Moroz. Thanks to Jim Bell for providing his telescopic spectra in the visible, to David Crisp for the synthetic atmospheric spectrum, to Ted Roush, James Orenberg, and Janice Bishop for their mineral spectra, and to Yves Langevin for

constructive discussions. The ISM data base will be distributed on CD by CNES; information about the instrument and data set is available at http://www.ias.fr/cdp/ISM.

REFERENCES

Banin, A., and L. Margulies 1983. Simulation of Viking biology experiments suggests smectites, not palagonites, as martian soil analogs. *Nature* **305,** 523–525.

Bell, J. 1992. Charge-coupled device imaging spectroscopy of Mars 2. Results and implications for martian ferric mineralogy. *Icarus* **100,** 575–597.

Bell, J. F., T. B. McCord, and P. D. Owensby 1990. Observational evidence of crystalline iron oxides on Mars. *J. Geophys. Res.* **95,** 14,447–14,462.

Bibring, J.-P., M. Combes, Y. Langevin, C. Cara, P. Drossart, T. Encrenaz, S. Erard, O. Forni, B. Gondet, L. V. Ksanfomaliti, E. Lellouch, P. Masson, V. I. Moroz, F. Rocard, J. Rosenqvist, C. Sotin, and A. Soufflot 1990. ISM observations of Mars and Phobos: First results. *Proc. Lunar Planet. Sci. Conf.* **20,** 461–471.

Bishop, J., and C. Pieters 1995. Low-temperature and low atmospheric pressure infrared reflectance spectra of Mars soil analog materials. *J. Geophys. Res.* **100,** 5369–5379.

Bishop, J., C. Pieters, R. Burns, J. Edwards, R. Mancinelli, and H. Fröschl 1995. Reflectance spectroscopy of ferric sulfate-bearing montmorillonites as Mars soil analog materials. *Icarus* **117,** 101–119.

Blaney, D. L., and T. B. McCord 1995. Indications of sulfate minerals in the martian soil from Earth-based spectroscopy. *J. Geophys. Res.* **100,** 14,433–14,441.

Calvin, W. M. 1997. Variations of the 3-μm absorption feature on Mars: Observations over eastern Valles Marineris by the Mariner 6 infrared spectrometer. *J. Geophys. Res.* **102,** 9097–9107.

Calvin, W. M., and T. King 1997. Spectral characteristics of Fe-bearing phyllosilicates: Comparison to Orgueil, Murchison and Murray. *Meteoritics Planet. Sci.* **32,** in press.

Calvin, W. M., T. V. V. King, and R. N. Clark 1994. Hydrous carbonates on Mars? Evidence from Mariner 6/7 infrared spectrometer and groundbased telescopic spectra. *J. Geophys. Res.* **99,** 14,659–14,675.

Chassefière, E., P. Drossart, and O. Korablev 1995. Post-Phobos model for the altitude and size distribution of dust in the low martian atmosphere. *J. Geophys. Res.* **100,** 5525–5539.

Clancy, R. T., S. W. Lee, G. R. Gladstone, W. W. McMillan, and T. Roush 1995. A new model for Mars atmospheric dust based upon analysis of ultraviolet through infrared observations from Mariner 9, Viking and Phobos. *J. Geophys. Res.* **100,** 5251–5263.

Clark, R. N., G. A. Swayze, R. B. Singer, and J. Pollack 1990. High resolution reflectance spectra of Mars in the 2.3 micron region: Evidence for the mineral scapolite. *J. Geophys. Res.* **95,** 14,463–14,480.

Cooper, C., and J. Mustard 1997. Loss of spectral contrast in hyperfine palagonite: Implications for smectite on Mars. In *Lunar and Planetary Science* Vol. XXVIII, pp. 257–258. Lunar and Planetary Institute, Houston. [Abstract]

Encrenaz, T., and E. Lellouch 1990. On the origin of weak absorption features in the infrared spectrum of Mars. *J. Geophys. Res.* **95,** 14,589–14,594.

Erard, S. 1995. Variability of surface materials in the equatorial regions of Mars. In *Lunar and Planetary Science* Vol. XXVI, pp. 379–380. Lunar and Planetary Institute, Houston. [Abstract]

Erard, S. 1997. *Technical Help for ISM Investigators. Documentation to the ISM/Phobos-2 Data Base.* IAS Technical Report T 97-01.

Erard, S., J.-P. Bibring, J. F. Mustard, O. Forni, J. W. Head, S. Hurtrez, Y. Langevin, C. M. Pieters, J. Rosenqvist, and C. Sotin 1991. Spatial variations in composition of the Valles Marineris and Isidis Planitia regions of Mars derived from the ISM data. *Proc. Lunar Planet. Sci. Conf.* **21,** 437–455.

Erard, S., J. Mustard, S. Murchie, J.-P. Bibring, P. Cerroni, and A. Coradini 1994. Effects of aerosols scattering on near-infrared observations of the martian surface. *Icarus* **111,** 317–337.

Gooding, J. L. 1992. Soil mineralogy on Mars: Possible clues from salts and clay in SNC meteorites. *Icarus* **99,** 28–41.

Hapke, B. 1993. *Theory of Reflectance and Emittance Spectroscopy*. Cambridge Univ. Press, New York.

Hunt, G. R., L. M. Logan, and J. W. Salisbury 1973. Mars: Components of infrared spectra and composition of the dust cloud. *Icarus* **18,** 459–469.

Jakosky, B. M., and C. B. Farmer 1982. The seasonal and global behavior of water vapor in the Mars atmosphere: Complete global results of the Viking atmospheric water detector experiment. *J. Geophys. Res.* **87,** 2999–3019.

Martin, T. Z. 1986. Thermal infrared opacity of the Mars atmosphere. *Icarus* **66,** 2–21.

McCord, T. B., R. N. Clark, and R. B. Singer 1982. Mars: Near-infrared spectral reflectance of surface regions and compositional implications. *J. Geophys. Res.* **87,** 3021–3032.

Moersch, J. E., and P. R. Christensen 1995. Thermal emission from particulate surfaces: A comparison of scattering models with measured spectra. *J. Geophys. Res.* **100,** 7465–7477.

Moroz, V. I. 1964. The infrared spectrum of Mars (1.1–4.1 μm). *Soviet Astron.* **8,** 273–281.

Moroz, V. I., E. V. Petrova, L. V. Ksanfomality, O. F. Ganpantzerova, N. V. Goroshkova, A. V. Zharkov, G. E. Nikitin, L. Esposito, J.-P. Bibring, M. Combes, and A. Soufflot 1991. Characteristics of aerosol phenomena in martian atmosphere from KRFM experiment data. *Planet. Space Sci.* **39,** 199–207.

Morris, R., D. Agresti, H. Lauer, J. Newcomb, T. Shelfer, and A. Murali 1989. Evidence for pigmentary hematite on Mars based on optical, magnetic and Mössbauer study of superparamagnetic (nanocrystalline) hematite. *J. Geophys. Res.* **94,** 2760–2778.

Murchie, S., J. F. Mustard, J. Bishop, J. Head, C. M. Pieters, and S. Erard 1993. Spatial variations in the spectral properties of bright regions on Mars. *Icarus* **105,** 454–468.

Mustard, J., and J. Bell 1994. New composite reflectance spectra of Mars from 0.4 to 3.14 μm. *Geophys. Res. Lett.* **21,** 353–356.

Mustard, J., S. Erard, J.-P. Bibring, J. W. Head, S. Hurtrez, Y. Langevin, C. M. Pieters, and C. J. Sotin 1993. The surface of Syrtis Major: Composition of the volcanic substrate and mixing with altered dust and soil. *J. Geophys. Res.* **98,** 3387–3400.

Mustard, J. F., and J. M. Sunshine 1995. Seeing through the dust: Martian crustal heterogeneity and links to the SNC meteorites. *Science* **267,** 1623–1626.

Pimentel, G. C., P. B. Forney, and K. C. Herr 1974. Evidence about hydrate solid water in the martian surface from the 1969 Mariner infrared spectrometer. *J. Geophys. Res.* **79,** 1623–1634.

Pollack, J. B., T. Roush, F. Witteborn, J. Bregman, D. Wooden, C. Stocker, O. B. Toon, D. Rank, B. Dalton, and R. Freedman 1990. Thermal emission spectra of Mars (5.4–10.5 μm): Evidence for sulphates, carbonates, and hydrates. *J. Geophys. Res.* **95,** 14,595–14,628.

Roush, T., E. Roush, R. Singer, and P. Lucey 1992. Estimates of absolute flux and radiance factor of localized regions of Mars in the (2–4 μm) wavelength region. *Icarus* **99,** 42–50.

Roush, T. L., D. L. Blaney, and R. B. Singer 1993. The surface composition of Mars as inferred from spectroscopic observations. In *Remote Geochimical Analysis: Elemental and Mineralogical Composition*

(C. M. Pieters, and P. A. Englert, Eds.), pp. 367–397. Cambridge Univ. Press, New York.

Salisbury, J. W., L. Walter, N. Vergo, and D. D'Aria 1991. *Infrared (2.1–25 μm) Spectra of Minerals*. John Hopkins Univ. Press, Baltimore.

Scott, D. H., and K. L. Tanaka 1986. *Geologic Map of the Western Equatorial Region of Mars, 1:15,000,000*. U. S. Geol. Surv. Misc. Inv. Ser. Map I-1802-A.

Singer, R. B. 1985. Spectroscopic observation of Mars. *Adv. Space Res.* **5,** 8/59–8/68.

Singer, R. B., and T. L. Roush 1983. Spectral reflectance properties of particulate weathered coatings on rocks: Laboratory modeling and applicability to Mars. *Proc. Lunar Planet. Sci. Conf. 14th, in J. Geophys. Res.* **88,** 708–709.

Singer, R. B., T. B. McCord, R. N. Clark, J. B. Adams, and R. L. Huguenin 1979. Mars surface composition from reflectance spectroscopy: A summary. *J. Geophys. Res.* **84,** 8415–8426.

Soderblom, L. 1992. The composition and mineralogy of the martian surface from spectroscopic observations: 0.3 μm to 50 μm. In *Mars* (H. Kieffer, B. Jakosky, C. Snyder, and M. Matthews, Eds.), pp. 557–597. Univ. of Arizona Press, Tucson.

Veverka, J., J. Goguen, S. Yang, and J. Elliot 1978. Near-opposition limb darkening of solids of planetary interest. *Icarus* **33,** 368–379.